JACS
JOURNAL OF THE AMERICAN CHEMICAL SOCIETY
Article
pubs.acs.org/JACS

The Chemical Arsenal of *Burkholderia pseudomallei* Is Essential for Pathogenicity

John B. Biggins,[†] Hahk-Soo Kang,[†] Melinda A. Ternei,[†] David DeShazer,[‡] and Sean F. Brady*[,†]

[†]Laboratory of Genetically Encoded Small Molecules, Howard Hughes Medical Institute, The Rockefeller University, 1230 York Avenue, New York, New York 10065, United States

[‡]Bacteriology Division, United States Army Medical Research Institute of Infectious Diseases, Fort Detrick, Frederick, Maryland 21702-5011, United States

Supporting Information

ABSTRACT: Increasing evidence has shown that small-molecule chemistry in microbes (i.e., secondary metabolism) can modulate the microbe–host response in infection and pathogenicity. The bacterial disease melioidosis is conferred by the highly virulent, antibiotic-resistant pathogen *Burkholderia pseudomallei* (*BP*). Whereas some macromolecular structures have been shown to influence *BP* virulence (e.g., secretion systems, cellular capsule, pili), the role of the large cryptic secondary metabolome encoded within its genome has been largely unexplored for its importance to virulence. Herein we demonstrate that *BP*-encoded small-molecule biosynthesis is indispensible for *in vivo BP* pathogenicity. Promoter exchange experiments were used to induce high-level molecule production from two gene clusters (MPN and SYR) found to be essential for *in vivo* virulence. NMR structural characterization of these metabolites identified a new class of lipopeptide biosurfactants/biofilm modulators (the malleipeptins) and syrbactin-type proteasome inhibitors, both of which represent overlooked small-molecule virulence factors for *BP*. Disruption of Burkholderia virulence by inhibiting the biosynthesis of these small-molecule biosynthetic pathways may prove to be an effective strategy for developing novel melioidosis-specific therapeutics.

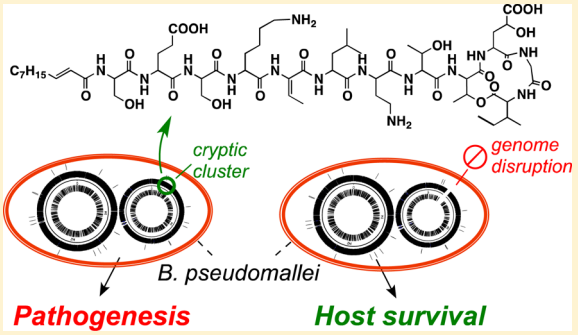

INTRODUCTION

Burkholderia pseudomallei (*BP*) is the causative agent for the bacterial septic disease melioidosis. Melioidosis is endemic throughout the tropical Southeast Pacific region and is considered a growing global health threat.[1] *BP*, an environmental saphrophyte by nature, is intrinsically resistant to multiple antibiotics due to factors including drug inactivation (e.g., β-lactamase activity), a multidrug efflux pump system, and an adaptive physiology that can alter drug target sites throughout disease progression.[2] As a result, mortality rates from melioidosis can approach ~50% even with antibiotic treatment.[3] Despite increased scrutiny in recent years, the mechanisms by which *BP* can establish and propagate an infection have remained unclear. Bioinformatics analyses of *BP* and its genetic relatives *Burkholderia mallei* (*BM*) and *Burkholderia thailandensis* (*BT*) indicate that substantial parts of their genomes are dedicated to polyketide (PK)- and nonribosomal peptide (NRP)-based secondary metabolism,[4−6] which we have hypothesized could be a key component of Burkholderia virulence.[7−9] While many of the gene clusters common to all three species have been studied, clusters that are solely found within the *BP* genome have remained uncharacterized, and to date, the specific roles that secondary metabolism has in establishing melioidosis have not been evaluated. Herein, we begin the characterization of the unique secondary metabolome encoded by *BP* and show that it is a key factor in melioid virulence. The importance of these molecules to *BP* pathogenicity suggests that inhibition of their biosynthesis could present a viable avenue for future therapeutic intervention.

Cryptic and/or silent small-molecule biosynthetic gene clusters are routinely found within sequenced bacterial genomes.[10] While biosynthetic gene clusters encoding molecules required for bacterial pathogenesis must be produced *in vivo* during an infectious event, many may remain silent in the laboratory setting due the lack of appropriate environmental stimuli needed to induce their activation (Figure 1). Due to its NIH/CDC Select Agent status, the manipulation of the *BP* genome for gaining access to silent biosynthesis has been cumbersome. As *BT* is generally considered to be avirulent in most mammalian hosts, it has been used as a convenient surrogate model to study biosynthesis in pseudomallei-group Burkholderia species.[7−9,11] As much of the *BP* secondary metabolome has been characterized through *BT*, neither the identity of the molecules encoded by *BP*-specific gene clusters nor the potential role these metabolites might play in virulence was known. Recently, the Schweizer group developed a *BP*

Received: May 10, 2014
Published: June 2, 2014

   dx.doi.org/10.1021/ja504617n | *J. Am. Chem. Soc.* 2014, 136, 9484−9490

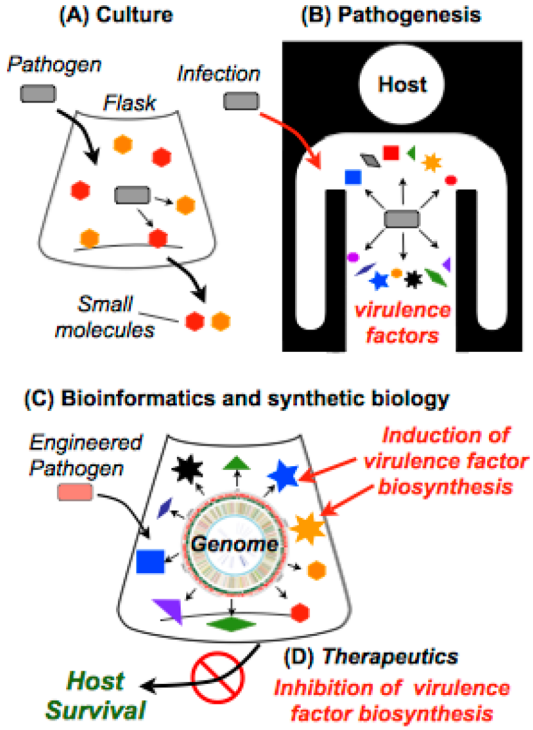

Figure 1. Examining the influence of secondary metabolism on bacterial pathogenicity. (A) Bacterial pathogens typically produce a limited number of metabolites under laboratory fermentation conditions, (B) while having the capacity to produce multiple metabolites within the context of an infection, which can function as virulence factors. (C) Cryptic/silent gene clusters can be identified bioinformatically in sequenced pathogen genomes. Through genome engineering, individual biosynthetic clusters can be both activated for accessing the encoded molecules and disrupted for determining their influence on bacterial pathogenicity. (D) Virulence factor biosynthesis can be targeted for the development of new disease-specific therapeutics.

adenine auxotroph (*Bp82*) that has been removed from the Select Agent list due to its inability to survive outside the laboratory,[12] providing a strain with the genetic background with which to study cryptic secondary metabolism of this important pathogen.

RESULTS AND DISCUSSION

A comparative genome analysis (Figure 2 and Table S1) of pseudomallei-group Burkholderia revealed that, although *BP*, *BM*, and *BT* share many PK/NRP gene clusters, three gene clusters are unique to *BP* (Figure 2; clusters 2, 14, and 15), and one cluster (cluster 11) is shared between *BP* and *BM* (but not *BT*). While extensively truncated versions of clusters 14 and 15 appear in the *BM* genome, cluster 2 is completely absent. Gene clusters 2 and 15 are predicted to encode for novel lipopeptides, cluster 11 is also predicted to encode a novel metabolite but has a gene organization and content similar to that found in the *BT*-specific thailandamide biosynthetic cluster,[13] and cluster 14 is predicted to encode a syrbactin-type structure (see discussion below) (Tables S1 and S2). We hypothesized that *BP*-specific cryptic gene clusters may play an important, and overlooked, role in melioidosis. To test this hypothesis, we used homologous recombination to delete the initial biosynthetic domains (detailed in Table S4) within the first either PK or NRP megasynth(et)ase gene of clusters 2, 11, 14, and 15, thereby creating four strains with individually disrupted biosynthetic gene clusters. This set of deletions was created in a fully sequenced clinical isolate, *B. pseudomallei 1026b* (*Bp1026b*), under strict BSL3 level biocontainment. These gene cluster disruption strains were then tested for pathogenicity using an intranasal murine infection model (Figure 3). Remarkably, disruption of any of the three gene

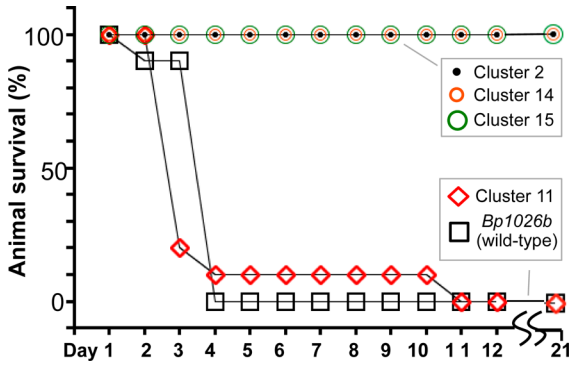

Figure 3. 21-day murine intranasal infection challenge of wild-type *BP* and the disruption mutants of biosynthetic clusters 2, 11, 14, and 15. The number of surviving mice is charted over time. Inoculum: 10^5 (10^6 for cluster 15) colony-forming units.

clusters that are uniquely found in *BP* (clusters 2, 14, and 15) completely abrogated *Bp1026b* murine virulence, even at titers up to 10 times the *Bp1026b* LD_{50} inoculum. Disruption of cluster 11, which is shared between *BP* and *BM*, led to a strain with virulence that was indistinguishable from the wild-type strain in the murine model. Each of the three NRP/PK metabolites encoded solely within the *BP* genome is therefore individually essential to the pathogenicity of this bacterium. Additionally, the growth rates of these three mutants were identical to that of wild-type *Bp1026b* (Figure S2), indicating

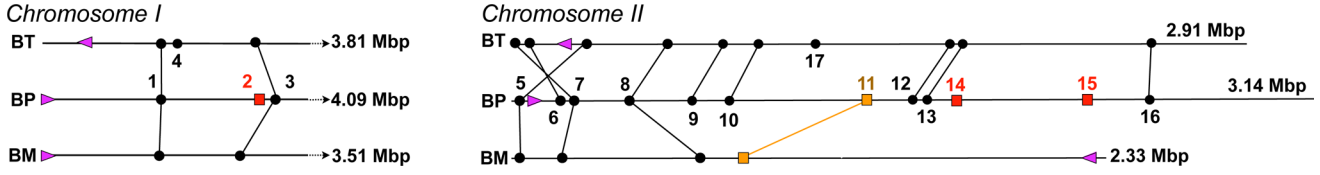

Figure 2. Comparison of the secondary metabolomes encoded by *B. pseudomallei 1026b* (*BP*), *B. mallei* ATCC 23344 (*BM*), and *B. thailandensis* E264 (*BT*). Positioning of individual NRP- and PK-encoding gene clusters within each genome is displayed. Clusters shared among the three species are indicated by the connective lines between genomes (detailed in Table S1). Genomes are linearized and arranged for clarity, with the purple arrowhead designating direction from the first gene in each chromosome (i.e., nucleotide + 1). Clusters 2, 14, and 15 (red) are unique to *BP*. Cluster 11 (yellow) is shared by *BP* and *BM* but absent in *BT*. Genes dedicated to NRP/PK-based secondary metabolism encompass approximately 6% of the *BP* genome.

dx.doi.org/10.1021/ja504617n | J. Am. Chem. Soc. 2014, 136, 9484−9490

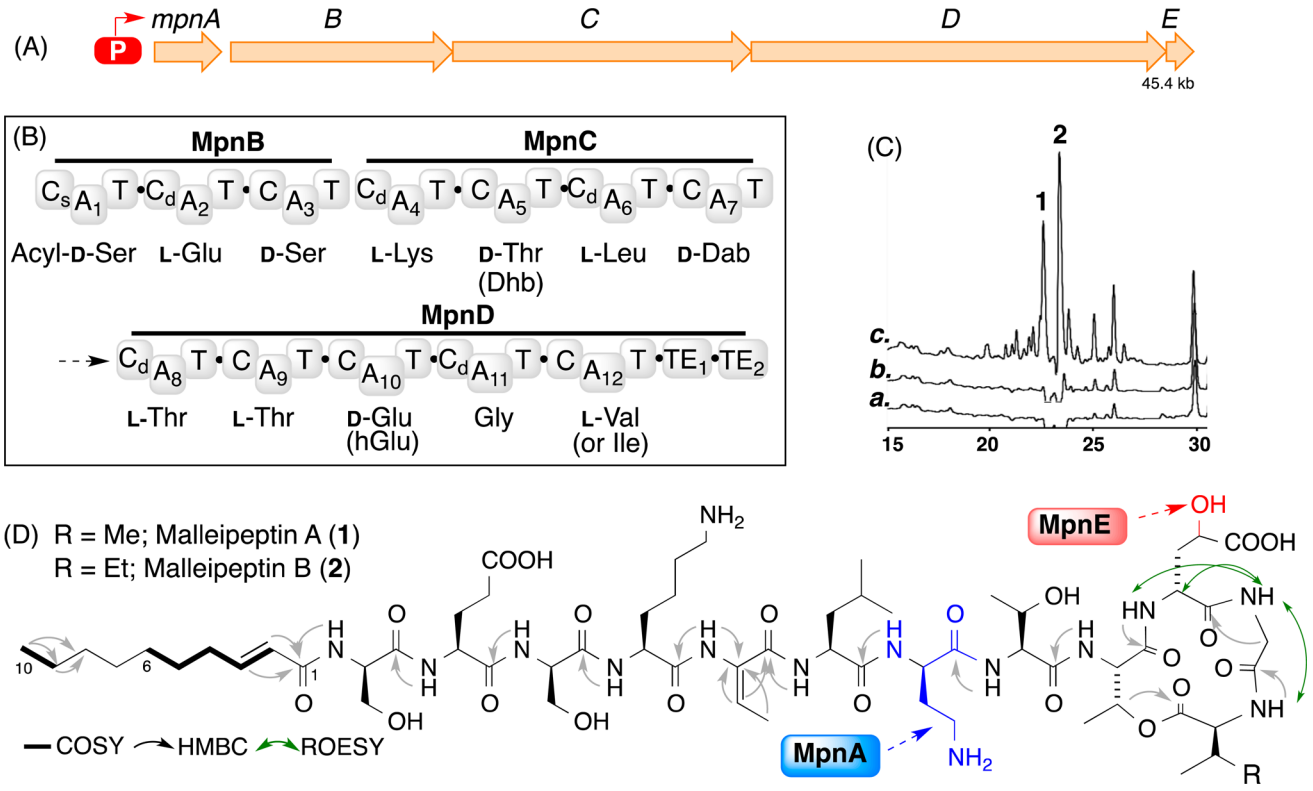

Figure 4. Characterization of the MPN cluster. (A) Biosynthetic gene cluster encoding the malleipeptins (genes *BP1026B_II1742-1746*, Table S2), with P_{RhaB} promoter exchange (red). (B) Predicted NRPS domain architecture and adenylation domain selectivity for MpnBCD. Parentheses indicate amino acids observed in the NMR-determined final malleipeptin structure that differ from the bioinformatics prediction. Abbreviations: C, condensation domain; C_S, starter condensation domain; C_d, dual condensation/epimerization domain; A, adenylation domain; T, peptidyl carrier domain; TE, thioesterase; Dhb, 2,3-dehydrobutyric acid; Dab, 2,4-diaminobutyric acid; hGlu, 4-hydroxyglutamic acid. (C) HPLC traces (diode array: 254 nm) of culture broth extracts from (*a*) *Bp82*, (*b*) *Bp82*:P_{RhaB}-MPN (no rhamnose), and (*c*) *Bp82*:P_{RhaB}-MPN (rhamnose induced). (D) Structure of malleipeptins A (**1**) and B (**2**) with key HMBC/ROESY correlations. Predicted tailoring enzyme functionalities (MpnA and MpnE) are highlighted. Comprehensive NMR assignments are detailed in Figure S3.

that the disruption of biosynthesis has no impact on general bacterial fitness. Based on their importance to *BP* virulence, we initiated the structural and functional characterization of the small molecules encoded by this collection of *BP*-specific gene clusters. Here we report on the characterization of two of these gene clusters. The third cluster (cluster 2), predicted to encode a five-amino-acid lipopeptide structure, has so far remained recalcitrant to characterization. Future studies will focus on activating this remaining silent gene cluster in the laboratory setting.

In previous work with *BT*, we developed a promoter-replacement strategy for up-regulating or activating secondary metabolite gene clusters in Burkholderia.[9] In this approach, the rhamnose-inducible promoter P_{RhaB} is inserted directly upstream of a key operon in a gene cluster of interest, providing a conditional switch that activates or represses biosynthesis in the presence or absence of rhamnose, respectively. To investigate cryptic virulence-associated secondary metabolism in *BP*, we created P_{RhaB} recombination cassettes targeting the promoters upstream of the most biosynthetic-rich operons found in each gene cluster of interest (i.e., clusters 2, 14, and 15). These cassettes were ligated into the allele replacement vector pEXKm5 for use in transformation, recombination, selection, and ultimately promoter replacement in *Bp82*.[14] Using this approach, we were able to induce high-level metabolite production from clusters 14 and 15 (SYR and MPN clusters, respectively), and then through a combination of bioinformatics, mass spectroscopy, and NMR, we characterized the molecules encoded by these two clusters, as follows.

On the basis of bioinformatics analysis, we predicted that the MPN gene cluster was composed of a unidirectional five-gene locus (*mpnA-E*). Three of these genes, *mpnBCD*, encode large modular NRP megasynthetases (NRPSs) that together are predicted to synthesize a 12-amino-acid peptide (Figure 4A). The MpnB initiation module is predicted to incorporate an acyl group as a starter unit, suggesting that the MPN cluster would encode a lipopeptide.[15] The two additional genes predicted to reside in the MPN cluster would appear to be responsible for generating unnatural amino acids for use by the NRPSs. The first, *mpnA*, encodes a diaminobutyrate-2-oxoglutarate transaminase that is commonly used in 2,4-diaminobutyric acid (Dab) biosynthesis, which is supported by the predicted Dab substrate binding specificity of one of the NRPS adenylation domains, A_7 (Figure 4B). The final gene, *mpnE*, is predicted to encode for a SyrP-like aspartic/glutamic acid hydroxylase.

The induction of MPN biosynthesis was achieved through P_{RhaB} insertion upstream of *mpnA* to give strain *Bp82*:P_{RhaB}-MPN. Upon induction with rhamnose, two major strain-specific metabolites appeared in culture broth extracts (Figure 4C; **1** and **2**, ESI $[M+H]^+$ m/z 1384.3 and 1398.2, respectively). These metabolites were absent in extracts from both wild-type *Bp82* and uninduced *Bp82*:P_{RhaB}-MPN cultures, indicating that, while the MPN cluster is critical for virulence *in vivo*, it remains silent under simple laboratory fermentation conditions.

dx.doi.org/10.1021/ja504617n | *J. Am. Chem. Soc.* 2014, 136, 9484−9490

Compounds **1** and **2** were purified by preparative reverse-phase chromatography from the methanol eluent of HP-20 resin-infused rhamnose-induced *Bp82*:P_{RhaB}-MPN cultures.

COSY/TOCSY analyses of major compound **2** showed 14 spin systems (Figures S3 and S4). On the basis of $^{1}H/^{13}C$ chemical shift data and HMQC/HMBC correlations, 12 of these are predicted to be amino acids. $^{1}H-^{13}C$ HMBC correlations between amide protons and adjacent carbonyl groups, with supporting $^{1}H-^{1}H$ ROESY correlations, defined the order of the 12 amino acids (Figures 4D and S3). Intramolecular cyclization through the threonine side chain (position 9) to form a 13-member macrolactone is supported by an HMBC correlation between the β-carbon methine proton (δ_H 5.37) of threonine and the carbonyl carbon of the C-terminal isoleucine residue ($\delta_{C\text{-}1}$ 169.2). The final two COSY spin systems are predicted to be part of an acyl substituent. An HMBC correlation between the carbonyl ($\delta_{C\text{-}1}$ 165.8) that is connected by HMBC correlations to the olefin-containing spin system and the serine amide proton (δ_H 8.24) confirms attachment of acyl group to the N-terminus. The *trans* geometry of the olefin was inferred from the large vicinal proton−proton coupling ($^{3}J_{HH}$ = 15 Hz). Ultimately, the exact length of the acyl substituent (2-(*E*)-decenoic) was determined on the basis of the molecular formula predicted by HRMS-TOF (*m*/*z* $[M+H]^+$ calcd for $C_{62}H_{105}N_{14}O_{22}$, 1397.7511; found, 1397.7528). Minor product **1** differs from **2** by CH_2, based on the MS-predicted formula (HRMS-TOF *m*/*z* $[M+H]^+$ calcd for $C_{61}H_{103}N_{14}O_{22}$, 1383.7372; found, 1383.7365). The same general NMR/MS arguments used to define the structure of **2** were used to establish the structure of **1**, with the exception that ^{1}H, ^{13}C, and both the COSY and TOCSY spectra indicate the C-terminal amino acid is a valine instead of an isoleucine. We have assigned these new lipopeptides the names malleipeptin A (**1**) and malleipeptin B (**2**).

Malleipeptins A and B are 12-amino-acid lipopeptides with a novel peptide sequence and a rarely seen 13-membered terminal lactone.[16,17] The primary malleipeptin amino acid sequence is in very good agreement with the bioinformatics prediction from the primary MpnBCD NRPS (Figures 4B). One exception is that 2,3-dehydro-2-aminobutanoic acid (Dhb), a dehydrated threonine residue, is incorporated at the position predicted to contain a threonine. The biosynthesis of the hydroxyglutamic acid (hGlu) moiety seen at position 10 is supported by the presence MpnE, which is a predicted SyrP-like aspartic/glutamic acid hydroxylase.[18] ^{1}H and COSY spectra with supporting $^{1}H-^{13}C$ HMQC correlations indicate that the oxidation occurs at the C-4 methine ($\delta_{C\text{-}4}$ 66.3), instead of the more common C-3 position (Figure S5). The presence of dual condensation/epimerization domains[19] in five of the NRPS modules indicates the incorporation of D-amino acids directly upstream of these domains at positions-1, −3, −5, −7, and −10 (Figure 4B), as is drawn in Figure 4D. The tandem thioesterases (TE_1·TE_2) found at the N-terminus of MpnD are commonly seen in large lipopeptide biosynthetic clusters and are predicted to encode for both intramolecular cyclization and proofreading to ensure the fidelity of the biosynthetic assembly line.[20,21] The malleipeptins are the first lipopeptides characterized from pseudomallei-group Burkholderia and are distinct from lipopeptides produced by unrelated Burkholderia species (e.g., burkholdine, occifungin).[22,23] The NRPSs responsible for the assembly of the malleipeptins do not align well to any deposited NRPS sequences outside of those found in other sequenced *BP* strains, indicating that the MPN cluster encodes for a novel structural family of lipopeptides that is so far solely associated with *BP* virulence.

The SYR cluster is comprised of nine genes (*syrA*−*I*) that are unidirectionally oriented (Figure 5A). Bioinformatics analysis

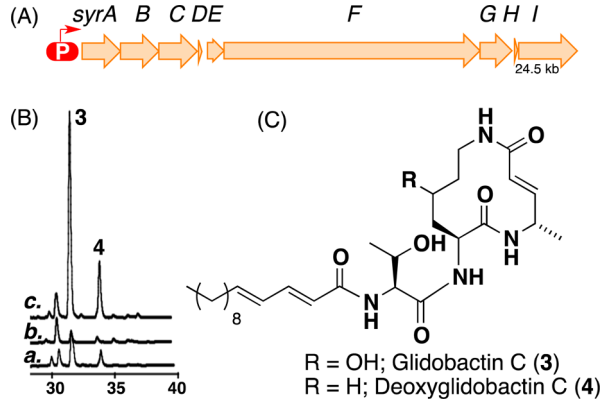

Figure 5. Characterization of SYR cluster. (A) Biosynthetic gene cluster encoding for the syrbactins (genes *BP1026B_II1345-1353*; Table S2) with P_{RhaB} promoter exchange (red). (B) HPLC traces (diode array: 254 nm) of culture broth extracts from (*a*) *Bp82*, (*b*) *Bp82*:P_{RhaB}-SYR (no rhamnose), and (*c*) *Bp82*:P_{RhaB}-SYR (rhamnose induced). (C) Structures of glidobactin C (**3**) and deoxyglidobactin C (**4**).

predicted this gene cluster was likely to encode a syrbactin-type proteasome inhibitor, as indicated by homologues of genes known to encode the hybrid PK/NRP syrbactin "warhead" that binds to the 20S proteasome active site (*syrEGFHI*).[24] In addition, this cluster is predicted to contain a set of genes (*syrABCD*) putatively responsible for synthesis and transfer of an acyl group (Figure S23). While syrbactins have been characterized from bacteria that are pathogenic to plant and insect hosts, this is the first syrbactin-type cluster identified within a mammalian pathogen. To study this cluster, we exchanged the promoter upstream of *syrA* with P_{RhaB}, yielding strain *Bp82*:P_{RhaB}-SYR. HPLC analysis of ethyl acetate extracts from rhamnose-infused cultures of *Bp82* and *Bp82*:P_{RhaB}-SYR showed a dramatic increase in two metabolites in the induced *Bp82*:P_{RhaB}-SYR cultures (Figure 5B; **3** and **4**). These metabolites are absent in extracts from uninduced *Bp82*:P_{RhaB}-SYR cultures, confirming the activation/repression phenotype provided by the P_{RhaB} promoter and coupling compound **3** and **4** production to SYR gene cluster induction. Compounds **3** and **4** were purified from ethyl acetate extracts using a modified Kupchan scheme followed by silica gel flash chromatography and preparative reverse-phase HPLC. MS and NMR data indicate that compound **3** is identical to the syrbactin glidobactin C (HRMS-TOF *m*/*z* $[M+Na]^+$ calcd for $C_{29}H_{48}N_4O_6Na$, 571.3514; found, 571.3483), which is characterized by the acylation of the PK/NRP warhead with a 2(*E*),4(*E*)-diene derivative of myristic acid (Figure 5C). The HRMS-predicted molecular formula for **4** differs from that of **3** by one oxygen atom (HRMS-TOF *m*/*z* $[M + Na]^+$ calcd for $C_{29}H_{48}N_4O_5Na$, 555.3522; found, 555.3520). ^{1}H and ^{13}C chemical shift data as well as COSY, HMQC, and HMBC correlation data indicate that compound **4** contains lysine, instead of 4-hydroxyllysine, within the warhead substructure. To our knowledge, this syrbactin variant, which we assign the name deoxyglidobactin C (**4**), has not been reported

dx.doi.org/10.1021/ja504617n | *J. Am. Chem. Soc.* 2014, 136, 9484−9490

previously. (Figure S23 details the biosynthetic rationale for compounds **3** and **4**.)

While syrbactins are known proteasome inhibitors, the biological activity of the malleipeptins was unknown. At the highest levels tested, the malleipeptins showed no general toxicity against bacterial (100 μg/disk) or human cells lines (100 μg mL^{-1}). A common function among non-cytotoxic lipopeptides is surfactant activity. In bacteria, biosurfactant production is thought to reduce the surface tension at water/hydrophobic interfaces, thereby helping to increase growth on surfaces; in pathogens, they have been shown to aid in bacterial invasion mechanisms.[25,26] Using a toluene emulsion assay, we tested the emulsive potential of *Bp82* and *Bp82*:P$_{RhaB}$-MPN cultures both in the presence and in the absence of rhamnose. Only the induced *Bp82*:P$_{RhaB}$-MPN supernatant formed any emulsion when mixed 1:1 with organic solvent, indicating that a potent surfactant property is, in fact, associated with malleipeptin production (Figure 6A). As biosurfactants have also been shown to possess a role in modulating biofilms,[16,26] we examined the effect of malleipeptin on *Bp82* biofilm production. At concentrations as low as 1 μM, malleipeptin disrupted *Bp82* biofilm formation (Figures 6B and S32). On the basis of these observations, we believe malleipeptins are biosurfactants that are required at some stage during *BP* infections.

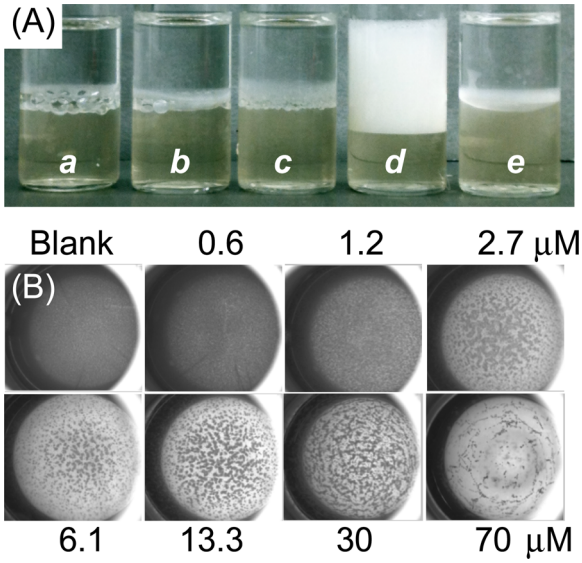

Figure 6. Malleipeptin activity. (A) Emulsification activity of cell culture supernatants. Equal parts toluene and supernatant were combined, vortexed, and then let stand for 2 h. (*a*) *Bp82*, no rhamnose; (*b*) *Bp82*, plus rhamnose; (*c*) *Bp82*:P$_{RhaB}$-MPN, no rhamnose; (*d*) *Bp82*:P$_{RhaB}$-MPN, plus rhamnose; (*e*) LB medium (blank). (B) Microtiter plate assay showing increasing disruption of *Bp82* top biofilm with increasing concentrations of **2** (200 μL cultures, 30 °C, 48 h; 20× magnification).

CONCLUSIONS

Comparative genome analyses led us to three small-molecule biosynthetic gene clusters that are required for *BP* pathogenicity. In a previous study involving *BT*, we showed that the lipophilic siderophore malleilactone, which is encoded by a gene cluster that is shared among *BP*, *BM*, and *BT* (Figure 2, cluster 8), strongly influences the virulence of *BT* in non-mammalian models.[9] Taken together, these works illustrate that small molecules play critical, yet largely overlooked, roles in Burkholderia pathogenesis (Figure 7). Additionally, the identification and characterization of small molecules encoded by cryptic gene clusters associated with virulence, especially when studying highly controlled Select Agent pathogens like *BP*, provide a means to potentially more safely dissect the detailed mechanisms of melioidosis.

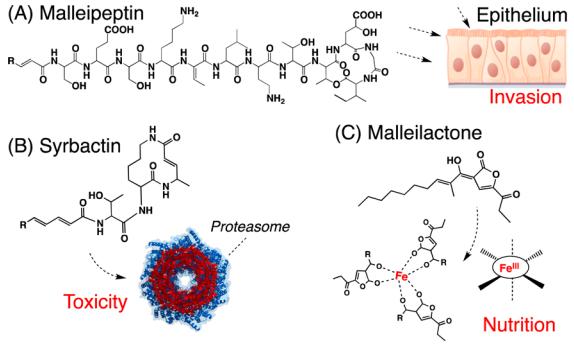

Figure 7. Putative metabolomics basis for bacterial virulence. Small-molecule biosynthesis is predicted to influence *BP* virulence through diverse mechanisms: (A) bacterial invasion, (B) systemic toxicity, and (C) acquisition of nutrients. The inhibition of these overlooked components of *BP* virulence should provide novel avenues for the development of *BP*-specific anti-infective agents.

As the pathogenicity of *BP* is known to involve intracellular replication following invasion of both epithelial and macrophage cells, potential roles for secondary metabolites within *BP* pathogenicity can be proposed. Biosurfactants have been shown to disrupt epithelial integrity, facilitate paracellular infiltration by bacterial pathogens, and support intercellular communication among bacteria by improving the solubility of lipophilic quorum sensing molecules.[25,27] The malleipeptins may play similar roles in *BP* pathogenicity, potentially aiding in bacterial infiltration and disease progression. Proteasome inhibition is known to directly activate programmed cell death through induction of apoptosis and autophagy across multiple cell lines, including macrophages.[28−31] In the context of *BP* infections, autophagy has been shown to be critical for diverting host nutrients to the pathogen.[32] Proteasome inhibition by the glidobactins could therefore provide the mechanistic explanation for both promoting intracellular replication or, in the case of macrophages, immunosuppression, which has long been suspected within *BP* pathogenicity.[33] In light of the importance of these small molecules to *BP* pathogenesis, the inhibition of their biosyntheses could prove to be a productive avenue for the development of next-generation therapeutics for combating melioidosis.

EXPERIMENTAL PROCEDURES

Construction of *B. pseudomallei* 1026b Mutants. Deletion of biosynthetic clusters was performed via a two-stage PCR strategy, wherein a key region of genomic DNA was excised by homologous recombination of DNA designed from genetic regions both upstream and downstream of the targeted excision region.[14] Upstream and downstream regions (~1 kb in length) were amplified from *Bp1026b* genomic DNA in a volume of 50 μL with 50 pmol of primer pair (primers 2F/2R and primers 3F/3R; listed in Table S3), 1X FailSafe PreMix E (Epicentre), and 5 U Phusion polymerase (NEB). PCR cycling conditions were as follows: 98 °C for 30 s, 30 cycles of 98 °C for 30 s; annealing at 62.5 °C for 30 s; 60 s extension at 72 °C; 72 °C, 1 min. Primers were designed to ligate into the *sacB*-based vector

dx.doi.org/10.1021/ja504617n | J. Am. Chem. Soc. 2014, 136, 9484−9490

pEXKm5[14] as a *Sma*I/*Xho*I cassette using the In-Fusion cloning kit (Clontech). Each fragment was gel purified with Qiagen PCR purification kit, and the fragments were ligated together into ∼2 kb fragments by a second round of PCR with the above protocol using primers 2F and 3R and ∼1 ng of each product from the initial PCR reaction. The extension time was increased to 2 min, with final 72 °C incubation at 2 min. This final product was then ligated into pEXKm5. Recombinant derivatives of pEXKm5 were electroporated into *E. coli* S17-1 and conjugated with *B. pseudomallei* for 8 h, as described elsewhere.[34] *Bp1026b* transconjugants were selected with kanamycin (1000 μg mL^{-1}), and polymyxin B (25 μg mL^{-1}) was used to counterselect *E. coli* S17-1. Optimal conditions for resolution of the *sacB* constructs were found to be LB agar lacking NaCl and containing 10% sucrose, with incubation at 25 °C for 3−4 days.

PCR Screening of Sucrose-Resistant Colonies To Identify Deletion Mutations. Colony PCR was performed by resuspending an isolated sucrose resistant colony in 50 μL of water and using 5 μL of the suspension in a PCR reaction. PCR amplifications were performed in a final reaction volume of 50 μL containing 1X FailSafe PreMix D (Epicentre), 1.25 U of FailSafe PCR Enzyme Mix (Epicentre), and 1 μM PCR primers. PCR cycling conditions were as follows: 97 °C for 5 min, 30 cycles of a three-temperature cycling protocol (97 °C for 30 s, 55 °C for 30 s, and 72 °C for 1 min); 72 °C, 10 min. Confirmation primers were designed to show a ∼500 bp region from the fusion of the upstream and downstream regions of the excised target locus, as verified by agarose gel (Figure S1).

BALB/c Mouse Virulence Studies. *B. pseudomallei* animal work was conducted under animal biosafety level 3 (ABSL3) conditions in accordance with Institutional Animal Care and Use Committee regulations at the U.S. Army Medical Research Institute of Infectious Diseases. Six- to eight-week-old female BALB/c mice (National Cancer Institute, Frederick, MD) were anesthetized with a 0.1−0.2 mL intraperitoneal injection of Ketamine HCl, Acepromazine, and Xylazine (K-A-X). The K-A-X solution was prepared by combining 5 mL of Ketamine HCl (100 μg mL^{-1}) and 0.5 mL of Acepromazine (10 μg mL^{-1}) with 2.75 mL of Xylazine (20 μg mL^{-1}) and mixing 1 mL of the resulting solution with 9 mL of saline. *B. pseudomallei* strains were grown overnight in Lennox LB broth and then serially diluted in phosphate-buffered saline, and 10^2−10^5 colony-forming units were used to inoculate groups of 10 mice by intranasal instillation. Briefly, 50 μL of the bacterial inoculum was gradually released into the nostrils of anaesthetized mice using a Gilson Pipetman P200. The infected animals were monitored daily for a period of 21 days, at which time the survivors were euthanized with CO_2, and the 50% lethal dose (LD_{50}) was calculated.

Promoter Exchange Cloning and *Bp82* Transformation. Avirulent *BP* strain, *Bp82*, was derived directly from *Bp1026b* through deletion of the Δ*purM* gene responsible for *de novo* adenine synthesis,[12] and all primers were based on the *Bp1026b* genome sequence. All media formulated for adenine auxotroph *Bp82* strain culturing were supplemented with adenine (80 μg mL^{-1}) and thymidine (5 μg mL^{-1}). For dual activation/suppression of individual biosynthetic gene clusters in *Bp82*, we previously designed a strategy for replacing native promoter regions upstream of an individual biosynthetic cluster with an inducible promoter imposing tight repression of transcription in Burkholderia (i.e., promoter exchange), detailed by Biggins et al.[9] Promoter exchange cassettes containing the rhamnose-inducible promoter P_{RhaB} and the *dhfr* trimethoprim resistance gene (from pSCrhaB2 vector),[35] flanked on each side by ∼1 kb of sequence homologous to the specific recombination sites in the Burkholderia genome, were constructed by successive rounds of PCR/restriction digest/ligation. Each ∼4.8 kb promoter exchange cassette was PCR amplified from its pUC-Rha parent clone with primer pair 2F/3R, gel purified, treated to afford blunt-ended phosphorylation (End-It DNA repair kit; Epicenter), and ligated into vector pEXKm5 at the CIP-treated *Sma*I site within the multicloning region. Each pEXKm5-cloned variant was transported into *E. coli* S17-1 and conjugated with *Bp82*, as described.[14] *Bp82*/*E. coli* co-cultures were resuspended in 250 μL of LB medium and selected over 2−3 days on selection media LB agar/kanamycin (1000 μg mL^{-1})/trimethoprim (100 μg mL^{-1}). Gentamycin (20 μg mL^{-1}) was also added to counterselect against *E. coli*. Merodiploid *Bp82* colonies were picked and restreaked on a fresh selection plate for 48 h. A single colony was then grown in 1 mL of YT medium[14] overnight and plated on *sacB*-curing media YT agar/trimethoprim (100 μg mL^{-1})/X-Gluc (50 μg mL^{-1})/15% sucrose for 2−3 days at 30 °C. Excision of the plasmid backbone was verified by white colony phenotype and the inability to survive against kanamycin (1000 μg mL^{-1}) selection. Proper recombinant transformants were verified for proper insertion/recombination by PCR using primer pair 4F/5R for proper ∼4.8 kb fragment containing P_{RhaB} and flanking hybridization domains. Seamless insertion of promoter P_{RhaB} was verified by amplifying the region within the P_{RhaB} promoter and downstream of the insertion site with primer pairs 5F/5R, gel purifying each ∼1 kb fragment, and Sanger sequencing to verify that no mutations occurred during the cloning process.

Strain-Specific Induction of Malleipeptin Production. Strain *Bp82*:P_{RhaB}-MPN was grown overnight to confluence in LB/trimethoprim (100 μg mL^{-1}), and then 500 μL was inoculated into 50 mL of LB/trimethoprim (100 μg mL^{-1})/0.2% L-rhamnose with 1.5 g of HP-20 resin added and incubated at 30 °C, 200 rpm, 72 h. An identical control culture lacked the addition of L-rhamnose to the culture medium. After 72 h, resin was filtered from the broths, washed twice in equal amounts of deionized water, and dried overnight in a laboratory fume hood. Dried resins were resuspended in 10 mL of methanol, sonicated, decanted, dried *in vacuo*, and monitored by reverse-phase HPLC-MS (linear gradient from 10:90 CH_3CN/H_2O with 0.1% formic acid to 100% CH_3CN with 0.1% formic acid over 50 min; 0.7 mL min^{-1}; Waters XBridge C18, 5 μm, 4.6 × 150 mm). Rhamnose-induced culture (illustrated in Figure 4C) displayed two major peaks (retention times: 22.6 min, **1**; 23.4 min, **2**) that are not present in the control cultures.

Strain-Specific Induction of Syrbactin Production. Strain *Bp82*:P_{RhaB}-SYR was grown overnight to confluence in LB/trimethoprim (100 μg mL^{-1}), and then 500 μL was inoculated into 50 mL of LB/trimethoprim (100 μg mL^{-1})/0.2% L-rhamnose and incubated at 30 °C, 200 rpm, 72 h. An identical control culture lacked the addition of L-rhamnose to the culture medium. After 72 h, 20 mL of culture broth was extracted with an equal amount of ethyl acetate, dried *in vacuo*, and monitored by reverse-phase HPLC-MS (linear gradient from 10:90 CH_3CN/H_2O with 0.2% trifluoroacetic acid to 100% CH_3CN with 0.2% trifluoroacetic acid over 50 min; 0.7 mL min^{-1}; Waters XBridge C18, 5 μm, 4.6 × 150 mm). Rhamnose-induced culture (illustrated in Figure 5C) displayed two major peaks (retention times: 31.6 min, **3**; 34.0 min, **4**) that are repressed in non-induced cultures.

Emulsion Assay. The emulsive potential of malleipeptin producing extracts of *Bp82*:P_{RhaB}-MPN cultures was tested against wild-type *Bp82*, both with (induction) and without 0.2% L-rhamnose added to media, using toluene as an organic solvent.[16] Confluent cultures of each strain were grown overnight from a freshly restreaked colony in LB medium. Aliquots of 50 μL of LB media, both with and without added 0.2% L-rhamnose, were inoculated with 500 μL of each strain and incubated (48 h, 200 rpm; 30 °C). One milliliter of each culture was pelleted (60 s; 15000*g*), from which 500 μL was mixed with an equal volume of toluene in a glass vial, vortexed vigorously, and rested for 2 h. LB media alone was used as a blank control.

Biofilm Disruption Assay. A confluent culture of *Bp82* was grown overnight from a freshly restreaked colony in LB medium, inoculated into 50 mL LB medium, and grown to OD_{600} 0.5 (200 rpm; 37 °C), after which the culture was diluted 1:100 and seeded in 96-well plates (200 μL/well). The concentration of purified malleipeptin B ranged from 100 μg mL^{-1} (70 μM) to 0.34 μg mL^{-1} (0.24 μM) (2.25-fold dilution increments). Blank controls (methanol solvent vector) were co-incubated in adjacent wells. Assays were done in triplicate. Cultures were incubated (48 h; 80 rpm; 30 °C), and top biofilm formations were visualized through a dissecting stereoscope. Disruption in biofilm is evident in cultures with ligand concentration above ∼1 μM malleipeptin B, wherein biofilms become increasingly porous and

dx.doi.org/10.1021/ja504617n | J. Am. Chem. Soc. 2014, 136, 9484−9490

fragmented. Still pictures were taken with a Leica M60 stereoscope affixed with an IC80HD camera (20× magnification).

■ ASSOCIATED CONTENT

Supporting Information

Experimental details and additional data. This material is available free of charge via the Internet at http://pubs.acs.org.

■ AUTHOR INFORMATION

Corresponding Author

sbrady@rockefeller.edu

Notes

The authors declare no competing financial interest.

■ ACKNOWLEDGMENTS

This work was supported by Northeast Biodefense Center (U54-A1057158, to S.F.B), NIH (GM077516, to S.F.B), and the Defense Threat Reduction Agency (DTRA)/Joint Science and Technology Office for Chemical and Biological Defense (JSTO-CBD, proposal no. CBCALL12-LS1-2-0070, to D.D.). Opinions, interpretations, conclusions, and recommendations are those of the authors and are not necessarily endorsed by the U.S. Army. We thank Eugene Blue for assistance in conducting the mouse experiments, and Steven Kern for statistical support. Strain *Bp82* was graciously provided to us Prof. Herbert Schweizer (Colorado State University). Support was provided by the following Resource Centers of The Rockefeller University: Proteomics (mass spectrometry) and High-Throughput and Spectroscopy (NMR facilities).

■ REFERENCES

(1) Galyov, E. E.; Brett, P. J.; DeShazer, D. *Annu. Rev. Microbiol.* **2010**, *64*, 495.

(2) Schweizer, H. P. *Future Microbiol.* **2012**, *7*, 1389.

(3) Limmathurotsakul, D.; Wongratanacheewin, S.; Teerawattanasook, N.; Wongsuvan, G.; Chaisuksant, S.; Chetchotisakd, P.; Chaowagul, W.; Day, N. P.; Peacock, S. J. *Am. J. Trop. Med. Hyg.* **2010**, *82*, 1113.

(4) Kim, H. S.; Schell, M. A.; Yu, Y.; Ulrich, R. L.; Sarria, S. H.; Nierman, W. C.; DeShazer, D. *BMC Genomics* **2005**, *6*, 174.

(5) Nierman, W. C.; et al. *Proc. Natl. Acad. Sci. U.S.A.* **2004**, *101*, 14246.

(6) Yu, Y.; et al. *BMC Microbiol.* **2006**, *6*, 46.

(7) Biggins, J. B.; Gleber, C. D.; Brady, S. F. *Org. Lett.* **2011**, *13*, 1536.

(8) Biggins, J. B.; Liu, X.; Feng, Z.; Brady, S. F. *J. Am. Chem. Soc.* **2011**, *133*, 1638.

(9) Biggins, J. B.; Ternei, M. A.; Brady, S. F. *J. Am. Chem. Soc.* **2012**, *134*, 13192.

(10) Challis, G. L. *J. Med. Chem.* **2008**, *51*, 2618.

(11) Liu, X.; Cheng, Y. Q. *J. Ind. Microbiol. Biotechnol.* **2014**, *41*, 275 and references therein.

(12) Propst, K. L.; Mima, T.; Choi, K. H.; Dow, S. W.; Schweizer, H. P. *Infect. Immun.* **2010**, *78*, 3136.

(13) Nguyen, T.; Ishida, K.; Jenke-Kodama, H.; Dittmann, E.; Gurgui, C.; Hochmuth, T.; Taudien, S.; Platzer, M.; Hertweck, C.; Piel, J. *Nat. Biotechnol.* **2008**, *26*, 225.

(14) Lopez, C. M.; Rholl, D. A.; Trunck, L. A.; Schweizer, H. P. *Appl. Environ. Microbiol.* **2009**, *75*, 6496.

(15) Rausch, C.; Hoof, I.; Weber, T.; Wohlleben, W.; Huson, D. H. *BMC Evol. Biol.* **2007**, *7*, 78 and references therein.

(16) Kuiper, I.; Lagendijk, E. L.; Pickford, R.; Derrick, J. P.; Lamers, G. E.; Thomas-Oates, J. E.; Lugtenberg, B. J.; Bloemberg, G. V. *Mol. Microbiol.* **2004**, *51*, 97.

(17) Neu, T. R. *Microbiol. Rev.* **1996**, *60*, 151.

(18) Strieker, M.; Nolan, E. M.; Walsh, C. T.; Marahiel, M. A. *J. Am. Chem. Soc.* **2009**, *131*, 13523.

(19) Balibar, C. J.; Vaillancourt, F. H.; Walsh, C. T. *Chem. Biol.* **2005**, *12*, 1189.

(20) Roongsawang, N.; Washio, K.; Morikawa, M. *Int. J. Mol. Sci.* **2010**, *12*, 141.

(21) Hou, J.; Robbel, L.; Marahiel, M. A. *Chem. Biol.* **2011**, *18*, 655.

(22) Lin, Z.; Falkinham, J. O., III; Tawfik, K. A.; Jeffs, P.; Bray, B.; Dubay, G.; Cox, J. E.; Schmidt, E. W. *J. Nat. Prod.* **2012**, *75*, 1518.

(23) Gu, G.; Smith, L.; Liu, A.; Lu, S. E. *Appl. Environ. Microbiol.* **2011**, *77*, 6189.

(24) Dudler, R. *Trends Microbiol.* **2014**, *22*, 28 and references therein.

(25) Zulianello, L.; Canard, C.; Kohler, T.; Caille, D.; Lacroix, J. S.; Meda, P. *Infect. Immun.* **2006**, *74*, 3134.

(26) Raaijmakers, J. M.; De Bruijn, I.; Nybroe, O.; Ongena, M. *FEMS Microbiol. Rev.* **2010**, *34*, 1037.

(27) Calfee, M. W.; Shelton, J. G.; McCubrey, J. A.; Pesci, E. C. *Infect. Immun.* **2005**, *73*, 878.

(28) Moran, E.; Carbone, F.; Augusti, V.; Patrone, F.; Ballestrero, A.; Nencioni, A. *Semin. Hematol.* **2012**, *49*, 270.

(29) Clerc, J.; Florea, B. I.; Kraus, M.; Groll, M.; Huber, R.; Bachmann, A. S.; Dudler, R.; Driessen, C.; Overkleeft, H. S.; Kaiser, M. *Chembiochem* **2009**, *10*, 2638.

(30) Archer, C. R.; et al. *Biochemistry* **2012**, *51*, 6880.

(31) Archer, C. R.; Koomoa, D. L.; Mitsunaga, E. M.; Clerc, J.; Shimizu, M.; Kaiser, M.; Schellenberg, B.; Dudler, R.; Bachmann, A. S. *Biochem. Pharmacol.* **2010**, *80*, 170.

(32) Singh, A. P.; Lai, S. C.; Nandi, T.; Chua, H. H.; Ooi, W. F.; Ong, C.; Boyce, J. D.; Adler, B.; Devenish, R. J.; Tan, P. *J. Bacteriol.* **2013**, *195*, 5487.

(33) Kalachev, I. I.; Baidus, A. N.; Ivanova, O. A.; Ganina, E. A.; Boldyrev, I. A.; Svetoch, E. A. *Vestn. Ross. Akad. Med. Nauk* **1997**, 32.

(34) DeShazer, D.; Brett, P. J.; Carlyon, R.; Woods, D. E. *J. Bacteriol.* **1997**, *179*, 2116.

(35) Cardona, S. T.; Valvano, M. A. *Plasmid* **2005**, *54*, 219.